

Analysis of sudden variations in photospheric magnetic fields during a large flare and their influences in the solar atmosphere

Brajesh Kumar¹, Ankala Raja Bayanna¹, Parameswaran Venkatakrishnan^{1,2} and Shibu Kuchandy Mathew¹

¹ Udaipur Solar Observatory, Physical Research Laboratory, Dewali, Badi Road, Udaipur 313 004, Rajasthan, India; brajesh@prl.res.in

² Indian Institute of Astrophysics, II Block, Koramangala, Bangalore 560 034, India

Received 2016 March 21; accepted 2016 May 1

Abstract The solar active region NOAA 11719 produced a large two-ribbon flare on 2013 April 11. We have investigated sudden variations in the photospheric magnetic fields in this active region during the flare by employing magnetograms obtained in the spectral line Fe I 6173 Å acquired by the Helioseismic and Magnetic Imager (HMI) onboard the *Solar Dynamics Observatory (SDO)* spacecraft. The analysis of the line-of-sight magnetograms from HMI show sudden and persistent magnetic field changes at different locations of the active region before the onset of the flare and during the flare. The vector magnetic field observations available from HMI also show coincident variations in the total magnetic field strength and its inclination angle at these locations. Using the simultaneous Dopplergrams obtained from HMI, we observe perturbations in the photospheric Doppler signals following the sudden changes in the magnetic fields in the aforementioned locations. The power spectrum analysis of these velocity signals shows enhanced acoustic power in these affected locations during the flare as compared to the pre-flare condition. Accompanying these observations, we have also used nearly simultaneous chromospheric observations obtained in the spectral line H α 6562.8 Å by the Global Oscillation Network Group (GONG) to study the evolution of flare-ribbons and intensity oscillations in this active region. The H α intensity oscillations also show enhanced oscillatory power during the flare in the aforementioned locations. These results indicate that the transient Lorentz force associated with sudden changes in the magnetic fields could drive localized photospheric and chromospheric oscillations, like the flare-induced oscillations in the solar atmosphere.

Key words: Sun: sunspots — Sun: flares — Sun: magnetic fields — Sun: oscillations — Sun: photosphere — Sun: chromosphere

1 INTRODUCTION

Solar flares are one of the most catastrophic events taking place in the solar atmosphere. During the flares, the magnetic energy stored in the corona is explosively released on short time scales (tens of minutes) in the form of thermal radiations in excess of 10^{32} erg and also produces energetic particles moving with very high speeds. The magnetic field configuration in the corona rapidly changes during the flares and signatures of these appear in the form of evolution of the photospheric magnetic fields. The changes in the photospheric magnetic fields during flares take place, both on short time scales of a few minutes during the impulsive phase of the flare and longer time scales of hours covering the phases before and after the flare. The rapid short-term magnetic field changes (magnetic transients) during flares were first reported by Patterson & Zirin (1981). However, it was interpreted later on (Patterson 1984; Harvey 1986) that the reported magnetic transients could be attributed to the transient emission

of the spectral line being used for measuring the magnetic fields. This interpretation was further advanced by Qiu & Gary (2003) through simulations of an observed transient polarity reversal in photospheric magnetic field measurements obtained by the Michelson Doppler Imager (MDI; Scherrer et al. 1995) onboard the *Solar and Heliospheric Observatory (SOHO)*; Domingo et al. 1995) spacecraft. On the other hand, Wang (1992) and Wang et al. (1994, 2002) reported rapid and permanent magnetic field changes in flaring active regions using the magnetic field observations at Big Bear Solar Observatory (BBSO). These observations were also confirmed by Kosovichev & Zharkova (2001) by analyzing the line-of-sight magnetograms obtained from the MDI instrument for an X-class flare on 2001 July 14. Later, Sudol & Harvey (2005) and Petrie & Sudol (2010) extensively analyzed changes in line-of-sight magnetic fields accompanying several X- and M-class flares in the different active regions. They showed abrupt, significant and permanent changes in the longitu-

dinal magnetic fields in the flaring active regions. These changes were typically observed to take place in less than 10 min with median magnitudes of 100 G. This sudden re-configuration of the magnetic fields during the flare produces Lorentz-force-transients in the solar atmosphere and is known as a “magnetic-jerk.” Hudson et al. (2008) and Fisher et al. (2012) estimated that the Lorentz force (with magnitude $\sim 10^{22}$ dynes) associated with the magnetic-jerks could be responsible for driving localized seismic waves in the solar photosphere. Kumar et al. (2011) found good correspondence between the enhanced localized photospheric velocity oscillations and the sites of magnetic-jerks observed in the solar active region NOAA 10930 during an X3.4-class flare on 2006 December 13. Since the magnetic field lines tied to the solar photosphere extend into the corona, it would be important to study the effect of magnetic-jerks simultaneously at the solar surface as well as in the higher layers of the solar atmosphere.

In this work, we present a detailed analysis of magnetic and velocity field changes associated with a large two-ribbon flare (of class M6.5) in the solar active region NOAA 11719 on 2013 April 11, using high-resolution and high-quality co-temporal full-disk photospheric magnetograms and Dopplergrams obtained from the Helioseismic and Magnetic Imager (HMI; Schou et al. 2012) instrument onboard the *Solar Dynamics Observatory* (*SDO*; Pesnell et al. 2012) spacecraft. Accompanying these observations, we have also used nearly simultaneous full-disk chromospheric $H\alpha$ observations of this flare event obtained from the Global Oscillation Network Group (GONG; Harvey & GONG Instrument Team 1995; Harvey et al. 1996) instrument in order to study the morphological and spatial evolution of the flare-ribbons as well as the $H\alpha$ intensity oscillations during the flare. The motivation of this work is to further investigate the influence of magnetic-jerks on localized photospheric velocity oscillations in the active region during this flare. We also aim to investigate possible variations in the chromospheric $H\alpha$ intensity oscillations corresponding to the photospheric locations of the magnetic-jerks in the active region during the flare. This would be useful for understanding the physical mechanism inter-linking different layers of the solar atmosphere.

In the following sections, we describe the observational data, our approach to the data analysis, the results, and the conclusions with a discussion.

2 THE OBSERVATIONAL DATA

The solar active region NOAA 11719 appeared on the eastern limb of the Sun on 2013 April 5 in the northern hemisphere and slowly it evolved into a very complex magnetic region (of class $\beta\gamma\delta$). It produced several C- and M-class flares during its passage on the solar disk. On 2013 April 11, a large two-ribbon flare (of class M6.5) occurred around 06:55 UT in this complex active region when it was located at the heliographic coordinates N10E08. The flare produced a high speed Earth-

directed coronal mass ejection (CME), type II radio bursts and protons with energy more than 10 MeV. Observations related to this interesting flare are available from various space- and ground-based observatories in different wavelengths and energies, viz., *SDO*, *Hinode* (Kosugi et al. 2007), *Solar TERrestrial RELations Observatory* (*STEREO*; Kaiser et al. 2008), *Geostationary Operational Environmental Satellite-15* (*GOES-15*), Nobeyama Radio Polarimeters (NoRP; Nakajima et al. 1985, and references therein), and GONG. In our analysis related to this flare, we employ the photospheric velocity and magnetic field observations obtained by the HMI instrument onboard *SDO*, chromospheric $H\alpha$ observations obtained from the GONG++ network (Harvey et al. 2011), and soft X-ray observations obtained from the *GOES-15* satellite during the flare event.

2.1 *SDO*/HMI Observations

The HMI instrument onboard the *SDO* spacecraft provides co-temporal, high quality full-disk photospheric Dopplergrams and line-of-sight magnetograms, taken in the Fe I 6173 Å line at the cadence of 45 s with a spatial sampling rate of ~ 0.5 arcsec per pixel. HMI derives the line-of-sight velocity and magnetic fields using the Stokes I and V measurements obtained by imaging spectro-polarimetry. The HMI instrument team also provides photospheric vector magnetograms at a cadence of 12 min using spectropolarimetric measurements of Stokes I , Q , U and V . In this study, we have used the tracked grid ($\sim 290 \times 193$ arcsec²) of magnetic maps and Doppler images of the active region NOAA 11719 for the period from 01:00 UT to 10:00 UT on 2013 April 11 to study changes associated with the flare in the photospheric magnetic and velocity fields in the active region. The HMI team produced the tracked data of the active region after remapping the region of interest onto heliographic coordinates. In addition to these images, we have also used continuum images of the active region as observed with HMI to study its morphology during the flare.

In Figure 1, we show the mean images of the active region NOAA 11719 in the continuum, the line-of-sight magnetic fields, and the total Doppler velocity constructed over the time period from 07:00 UT to 08:50 UT on 2013 April 11. It is clearly seen in these images that this active region had a very complex morphology, and hence this is the reason that it produced several flares during its journey through the solar disk.

2.2 GONG++ $H\alpha$ Observations

The network of GONG instruments was upgraded to GONG+ (Harvey et al. 1998) by replacing existing CCD cameras with a size of 256×256 pixels with a new CCD cameras having 1024×1024 pixels for better full-disk spatial resolution in the Dopplergrams, line-of-sight magnetograms, and continuum images acquired by these telescopes. Later on in mid-2010, GONG+ was upgraded to

GONG++ with the addition of the $H\alpha$ image acquisition system to provide a nearly continuous solar activity patrol for use in space weather applications (Harvey et al. 2011). Since then, the GONG++ network has obtained very useful full-disk chromospheric observations in the $H\alpha$ 6562.8 Å line at the cadence of one minute and spatial sampling of ~ 1.0 arcsec per pixel. The GONG++ network nicely covered the full event of this large two-ribbon flare in $H\alpha$ along with its other regular observations.

In Figure 2, we show the evolution of the flare-ribbons in $H\alpha$ using the GONG++ observations (negative images). Here, we notice that the flare-ribbons covered the umbra of the sunspot as the flare progressed and also that it was a long duration flare event. We have used these $H\alpha$ observations simultaneously with the aforementioned HMI observations to study the co-temporal photospheric and chromospheric changes associated with this flare.

2.3 GOES-15 Soft X-ray Observations

In order to understand the evolution of this flare in the solar environment, we also require information related to time evolution of high energy radiations from the Sun during the flare. In hard X-ray observations, the *Reuven Ramaty High Energy Solar Spectroscopic Imager (RHESSI;* Lin et al. 2002) satellite missed completely covering the impulsive phase of the flare. However, observations of the *GOES-15* satellite in soft X-ray emissions during the flare are available for nearly the full event. Hence, we have used the disk-integrated soft X-ray data in the 1–8 Å band from the *GOES-15* satellite because they have temporal information related to the emission of high-energy radiations from the Sun during the flare event.

In Figure 3, we show the temporal evolution of the light curves obtained from *GOES-15* in the 1–8 Å band and the $H\alpha$ (6563 Å line) flare-ribbons obtained from the GONG++ network. Here, we observe that both the high-energy light curves peak around 07:15 UT during the flare event. It is also noticed that *GOES-15* observations have a gap of nearly 20 min during the declining phase of the flare, which would hardly affect our study.

3 ANALYSIS AND RESULTS

The chief motivation of this work is to investigate any sudden variations in the line-of-sight photospheric magnetic fields in the localized regions of the active region during the flare and their influence on the localized velocity oscillations on the solar surface. We are also interested in examining the effect of these magnetic-jerks in the solar atmosphere. For this purpose, we have employed co-temporal high resolution photospheric magnetic and velocity field observations from the HMI instrument onboard the *SDO* spacecraft and nearly simultaneous chromospheric observations in $H\alpha$ from the GONG++ network. Details on the data reduction and analysis are presented as follows:

3.1 Analysis of Magnetic Field Changes in the Active Region Using HMI Data

We have analyzed the sequence from the tracked grid of photospheric line-of-sight magnetic images from HMI for the period from 06:00 UT to 10:00 UT on 2013 April 11 obtained at the cadence of 45 s, in order to search for sudden changes in the line-of-sight magnetic fields (B_{los}) in the active region during the flare. The field-of-view of the grid of tracked images is $\sim 290 \times 193$ arcsec² and it mostly covers the active region. It can be noted that the flare started around 06:55 UT and peaked around 07:15 UT on 2013 April 11 as seen in the light curves of soft X-ray observations from *GOES-15* and $H\alpha$ observations from GONG++ (c.f., Fig. 3). Hence, the analysis of magnetic fields during the period from 06:00 UT to 10:00 UT would be helpful in the study of magnetic-jerks, if there are any, in the active region during the flare as the aforementioned time period is comprised of the observations before and spanning the flare. We have scanned all the pixels in the field-of-view of the grid of tracked line-of-sight magnetic images for the detection of sudden changes in B_{los} in the active region. The following selection criteria have been applied to these magnetic images for identifying such locations in the active region:

(i) Considering that the noise level in the measurement of B_{los} made by the HMI instrument is less than 10 G per pixel, we have considered only those pixels whose average B_{los} over a grid of 3×3 adjoining pixels is more than ± 50 G in the given time series.

(ii) The extensive analysis of abrupt changes in longitudinal magnetic fields during several major flares done by Sudol & Harvey (2005) shows that the typical value of the abrupt changes in B_{los} is about 90 G observed during those flares. Following this, we have considered only those pixels where the difference between the maximum and minimum of the average B_{los} over a grid of 3×3 adjoining pixels in the time series is more than 100 G, separately, for the positive and negative magnetic field regions.

(iii) In order to eliminate the long-term slow variations and trends in the B_{los} in the sorted pixels with the aforementioned criteria, their time series of average B_{los} over a grid of 3×3 adjoining pixels is subjected to a $\tilde{\chi}^2$ test by applying a linear fit to the aforementioned time series. It is seen that the time series with a relatively high $\tilde{\chi}^2$ value shows fast variations in B_{los} . This criterion eliminates the pixels showing slow field evolution with time, and thus we are left with only those time series which have ‘step-like changes’ in B_{los} spanning the flare event.

(iv) Sudol & Harvey (2005) suggest that the abrupt changes in B_{los} typically occur in less than 10 min while Petrie & Sudol (2010) suggest that the median duration of abrupt field changes is about 15 min. Hence, to further distinguish between normal field evolution and abrupt and persistent changes in the B_{los} spanning the flare event, we have considered only those pixels where there is more than a 100 G change in average B_{los} over a grid of 3×3 adjoining pixels in less than 20 min.

Using the above mentioned criteria, we found six locations in the active region where we observe a group of pixels showing sudden and persistent changes in the B_{los} around the impulsive phase of the flare. These locations are shown as ‘K1’, ‘K2’, ‘K3’, ‘K4’, ‘K5’ and ‘K6’ as indicated by yellow circles in Figure 4. From this figure, we observe that these locations are situated in the vicinity of the $H\alpha$ flare-ribbons as well as away from the flare-ribbons. In the left panels of Figure 5, we have plotted the average values of B_{los} over a raster of 3×3 pixels in the aforementioned locations along with the light curve from *GOES-15*. A raster of 3×3 pixels is considered in order to avoid the possible errors in tracking of the grid of images. The centroids of these rasters in the different locations are shown by blue crosses in Figure 4. The Carrington heliocentric longitudes and latitudes (in degrees) of the aforementioned centroids are as follows: K1(76.91, 12.67), K2(74.06, 9.88), K3(73.49, 12.10), K4(73.64, 14.95), K5(68.75, 14.05) and K6(68.21, 17.26).

In the plots of B_{los} in Figure 5, we observe in most of the cases that the value of the longitudinal magnetic fields in the aforementioned locations changes abruptly, then maintains the new value for a period of time that is significantly longer than the duration of the sudden changes in B_{los} , and then shows unsteady behavior. Thus, these abrupt changes in B_{los} in our observations are “persistent” but not “permanent” changes in longitudinal magnetic fields as reported earlier by Sudol & Harvey (2005) and Petrie & Sudol (2010) for other flare events. It can also be noted that the sudden changes in B_{los} appear before the onset of a flare as well as during the flare event, and these changes are seen mostly in the weak to moderate magnetic field locations ($B_{\text{los}} < 500$ G) in the active region. The amount of change in B_{los} ranges between 100 G and 200 G taking place within time scales of 10 min as evident from the plots shown in Figure 5.

In order to understand the cause behind such variations in B_{los} , we have studied the morphological evolution of B_{los} at the locations ‘K1’, ‘K2’, ‘K3’, ‘K4’, ‘K5’ and ‘K6’ in the active region during the flare.

In Figure 6, we show the mosaic of the time evolution of B_{los} over a grid of 15×15 pixels containing the raster of 3×3 pixels at its center (enclosed by a white box) corresponding to the locations K1(76.91, 12.67), K2(74.06, 9.88), K3(73.49, 12.10), K4(73.64, 14.95), K5(68.75, 14.05) and K6(68.21, 17.26) in the active region for the period from 06:30 UT to 08:18 UT in the time interval of 12 min. The time duration from 06:30 UT to 08:18 UT covers the pre-flare phase and the flare phase. In this illustration of the morphological evolution of B_{los} , we observe fast changes in the magnetic concentrations in these affected locations. We conjecture that the sudden changes in B_{los} observed at the aforementioned locations could be due to the process of fast re-organization of the coronal magnetic fields during the flare, thereby producing fast changes in the directions of the photospheric magnetic fields.

We have also used the tracked vector magnetic field data available from HMI at a cadence of 12 min for the period from 06:00 UT to 10:00 UT on 2013 April 11, in order to study variations in the total magnetic field strength (B_0) and the inclination angle (γ) of the magnetic field lines at the locations of sudden changes seen in B_{los} in the active region. These data are co-aligned with the main grid of B_{los} images ($\sim 290\times 193$ arcsec²) for estimating B_0 and γ at the affected locations.

In Figure 7, we show the plots of B_0 and γ averaged over the same rasters of 3×3 pixels at the locations K1(76.91, 12.67), K2(74.06, 9.88), K3(73.49, 12.10), K4(73.64, 14.95), K5(68.75, 14.05) and K6(68.21, 17.26) in the active region as considered for B_{los} (c.f., Fig. 5) for the period from 06:00 UT to 10:00 UT on 2013 April 11. Here, we notice that both B_0 and γ show sudden and persistent variations around the time of the sudden changes seen in B_{los} . This implies that the sudden and persistent changes seen in B_{los} are due to the simultaneous sudden changes in B_0 and γ at the locations ‘K1’, ‘K2’, ‘K3’, ‘K4’, ‘K5’ and ‘K6’ in the active region.

These sudden changes in the magnetic fields at the aforementioned locations would produce Lorentz-force-transients or the “magnetic-jerk” in these affected areas.

3.2 Analysis of Velocity Field Changes in the Active Region Using HMI Data

The co-temporal full-disk photospheric Dopplergrams and line-of-sight magnetograms obtained by HMI provide an excellent opportunity to examine changes in the velocity signals associated with the sites of magnetic-jerks (‘K1’, ‘K2’, ‘K3’, ‘K4’, ‘K5’ and ‘K6’) in the active region. Therefore, we have analyzed the sequence of the tracked grid ($\sim 290\times 193$ arcsec²) of Doppler velocity images from HMI for the period from 06:00 UT to 10:00 UT on 2013 April 11 at a cadence of 45 s. In our analysis, we have studied the temporal evolution of the mean velocity signals from the aforementioned images over the same grids of 3×3 pixels at the centroid of the sites of magnetic-jerks in the active region with the Carrington heliocentric longitudes and latitudes (in degrees) as follows: K1(76.91, 12.67), K2(74.06, 9.88), K3(73.49, 12.10), K4(73.64, 14.95), K5(68.75, 14.05) and K6(68.21, 17.26).

In the right panels of Figure 5, we have plotted these mean line-of-sight velocity signals for the period from 06:00 UT to 10:00 UT on 2013 April 11 after removing the large background gradient in the observational data appearing mainly due to the orbital velocity of the satellite. Here, we observe significant perturbations in the photospheric Doppler signals following the epochs of the sudden and persistent changes seen in B_{los} in the aforementioned locations of the active region during the flare. The signature of enhancements seen in the velocity signals associated with these sites of magnetic-jerks motivated us to perform a power spectral analysis of these velocity varia-

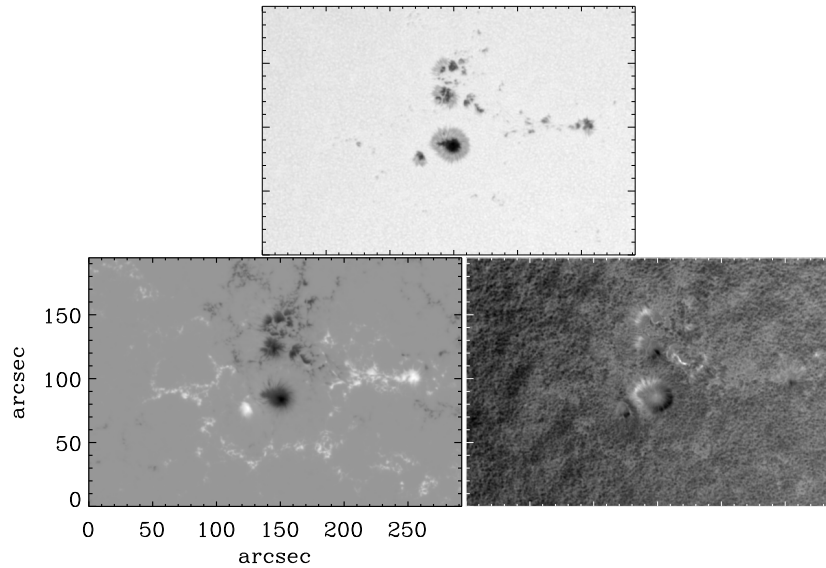


Fig. 1 Images of the active region NOAA 11719 in the continuum intensity (*top panel*), the line-of-sight photospheric magnetic fields (*bottom left panel*), and the photospheric Doppler velocity (*bottom right panel*) as observed with the HMI instrument onboard the *SDO* spacecraft. All the images shown here are the mean images constructed over the time interval 07:00–08:50 UT spanning the flare on 2013 April 11.

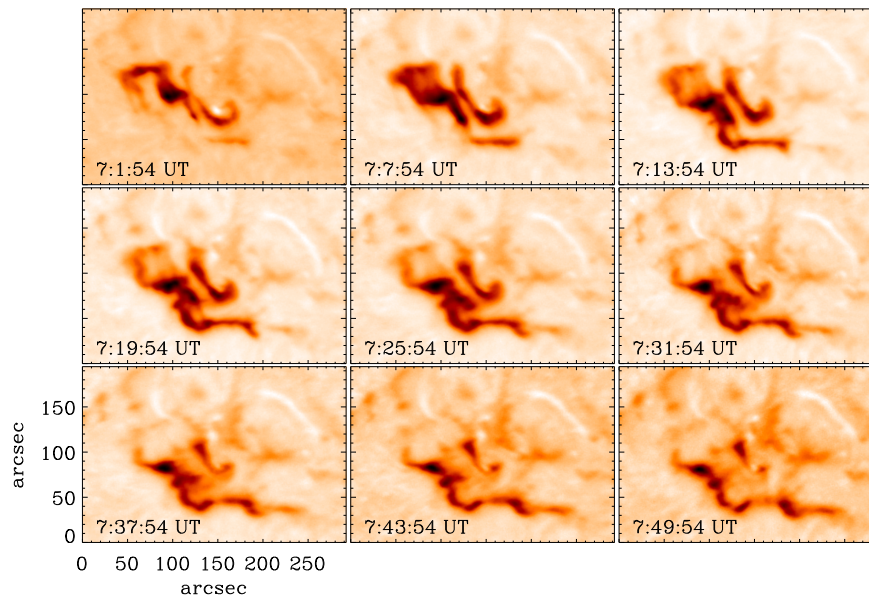


Fig. 2 Mosaic of images showing the evolution of the flare-ribbons in the $H\alpha$ 6563 Å line during the period 07:01:54–07:49:54 UT on 2015 April 11 using the GONG++ observations. Here, we notice that this was a two-ribbon flare and the flare-ribbons separated apart and covered the umbra of the sunspot as the flare progressed. The images are shown in negative for better appearance of the morphology of the flare-ribbons.

tions during the pre-flare phase (01:00–05:00 UT) and the flare phase (06:00–10:00 UT) covering the magnetic-jerks. Therefore, we applied a Fourier transform to these line-of-sight velocity signals from each individual pixel in the grid of 3×3 pixels and then an average power spectrum of velocity oscillations is constructed for each of the aforementioned rasters in the locations ‘K1’, ‘K2’, ‘K3’, ‘K4’, ‘K5’ and ‘K6’ in the active region for the pre-flare phase

and the flare phase. In Figure 8, we show in the black lines the average power spectra of velocity oscillations for the aforementioned locations in the active region for pre-flare and flare conditions. A smoothing fit (Savitzky-Golay Fit; Press et al. 1992) is applied (shown in the red lines) to these original power spectra for estimating the power envelopes.

It is evident from these velocity power spectra that there is an enhancement of the power of velocity oscilla-

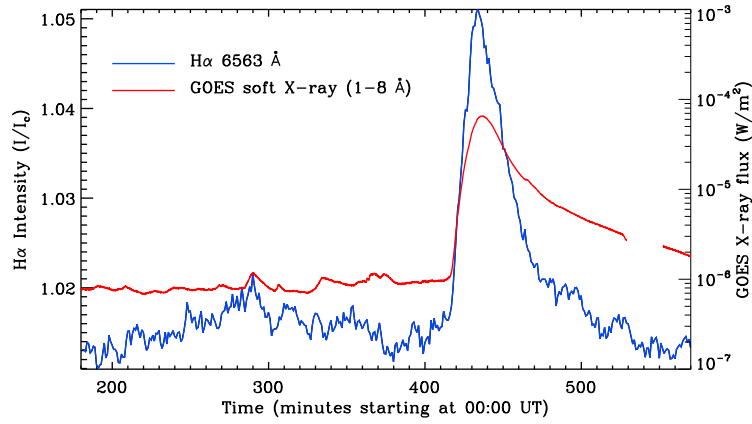


Fig. 3 Plots showing the temporal evolution of the light curves obtained from *GOES-15* in the 1–8 Å band and the H α (6562.8 Å line) flare-ribbons obtained from the GONG++ instrument during the period 03:00–09:30 UT on 2013 April 11. Here, we observe that both the high-energy light curves peak around 07:15 UT during the flare event. It is also noticed that *GOES-15* observations have a gap of nearly 20 min during the declining phase of the flare.

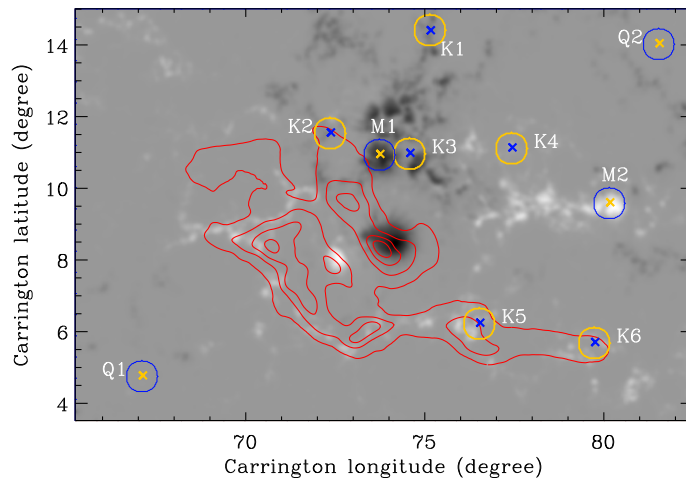


Fig. 4 The background shows the mean line-of-sight photospheric magnetic fields for the period 07:00–08:50 UT on 2013 April 11 in the active region NOAA 11719, as measured in the Fe I 6173 Å line by the HMI instrument onboard the *SDO* spacecraft. The overlaid contours shown in red are the locations of the chromospheric H α (6562.8 Å line) flare-ribbons averaged over the period 07:00–08:50 UT on 2013 April 11 in the aforementioned active region during an M6.5 class flare, as observed with the GONG++ instrument. The contours are drawn at the levels 90%, 80%, 70% and 60% of the maximum brightness in H α , from the center of the ribbons, respectively. The crosses shown in blue within the yellow circles (labeled as ‘K1’, ‘K2’, ‘K3’, ‘K4’, ‘K5’ and ‘K6’) are the centroids of the locations where we observe sudden and persistent changes in the line-of-sight photospheric magnetic fields (B_{los}) in the active region during the flare. Here, it is evident that these locations are in the vicinity of the flare-ribbons and away from the flare-ribbons in the active region. The crosses shown in yellow within blue circles (labeled as ‘M1’ and ‘M2’) are the centroids of the locations where we observe a gradual evolution of B_{los} during the flare whereas those labeled ‘Q1’ and ‘Q2’ are in the quiet Sun. The field-of-view is $\sim 290 \times 193$ arcsec².

tions in the 2–5 mHz band in the aforementioned locations during the flare as compared to the pre-flare condition. In this context, it is worth mentioning that if the magnitude of the magnetic flux of the selected region changes, this would affect the amplitude of velocity oscillations in those regions leading to a change in power of acoustic spectra. Thus, if there is a gross decrease in the magnitude of magnetic flux in the selected region during the flare, the velocity power spectra would show an increase of power with respect to that in the pre-flare condition and vice-

versa. Hence, the method of comparing the pre-flare velocity power spectrum with respect to that estimated during the flare may lead to erroneous interpretations. Therefore, we have checked the magnitude of B_{los} averaged over the aforementioned grids of 3×3 pixels in the locations ‘K1’, ‘K2’, ‘K3’, ‘K4’, ‘K5’ and ‘K6’ during the pre-flare and flare epochs considered in our analysis. It is seen that there is a gross increase in the magnitude of average B_{los} in the locations ‘K1’ and ‘K3’ while there is a gross decrease in the magnitude of average B_{los} in the locations ‘K2’, ‘K4’,

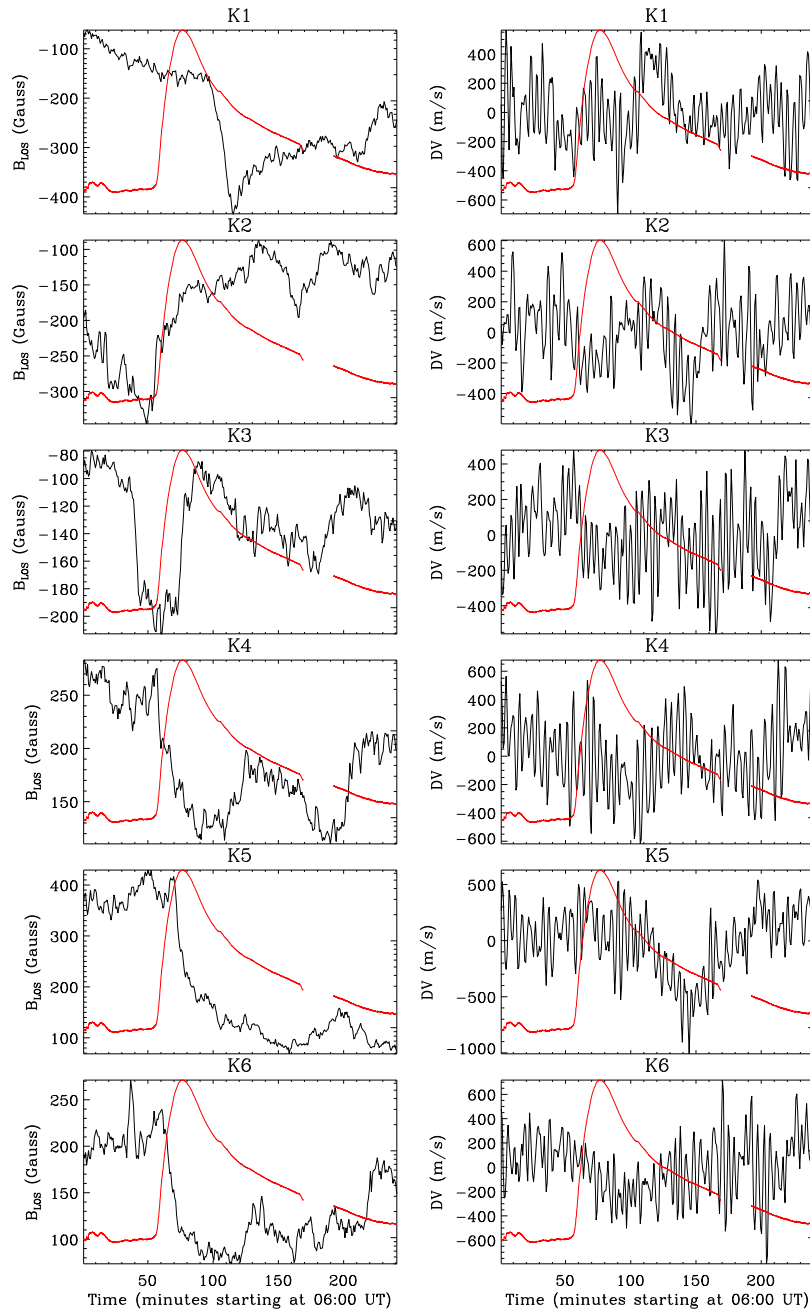


Fig. 5 Plots shown in black lines in the left panels represent the time evolution of the total line-of-sight photospheric magnetic field (B_{los}) averaged over a raster of nine pixels in the locations ‘K1’, ‘K2’, ‘K3’, ‘K4’, ‘K5’ and ‘K6’ in the active region during the period 06:00–10:00 UT on 2013 April 11 at the cadence of 45 s. Similarly, plots shown in black lines in the right panels represent time evolution of the simultaneous Doppler velocity (DV) in the aforementioned locations after removing the large background gradient due to orbital velocity of the satellite. The B_{los} and DV measurements are from HMI. The plots shown in red lines represent the evolution of soft X-ray flux in the energy band of 1–8 Å from *GOES-15*. The B_{los} in these locations shows sudden and persistent changes during the flare, which are followed by the perturbations in the DV at these locations.

‘K5’ and ‘K6’ during the flare phase as compared to the pre-flare phase. Also, it can be noted that ‘K1’ and ‘K3’ are much further away from the flare-ribbons. However, we observe an enhancement in the power of velocity oscillations in all the locations ‘K1’, ‘K2’, ‘K3’, ‘K4’, ‘K5’ and ‘K6’. This implies that the effect of “magnetic-jerk” dominates the effect of the normal evolution of magnetic

concentrations in the aforementioned locations concerning the enhancement of the power of the velocity oscillations in these identified locations.

In order to further verify our aforementioned observations and the related interpretations, we have done a similar analysis for some other locations in and around this active region for the pre-flare phase and the flare phase.

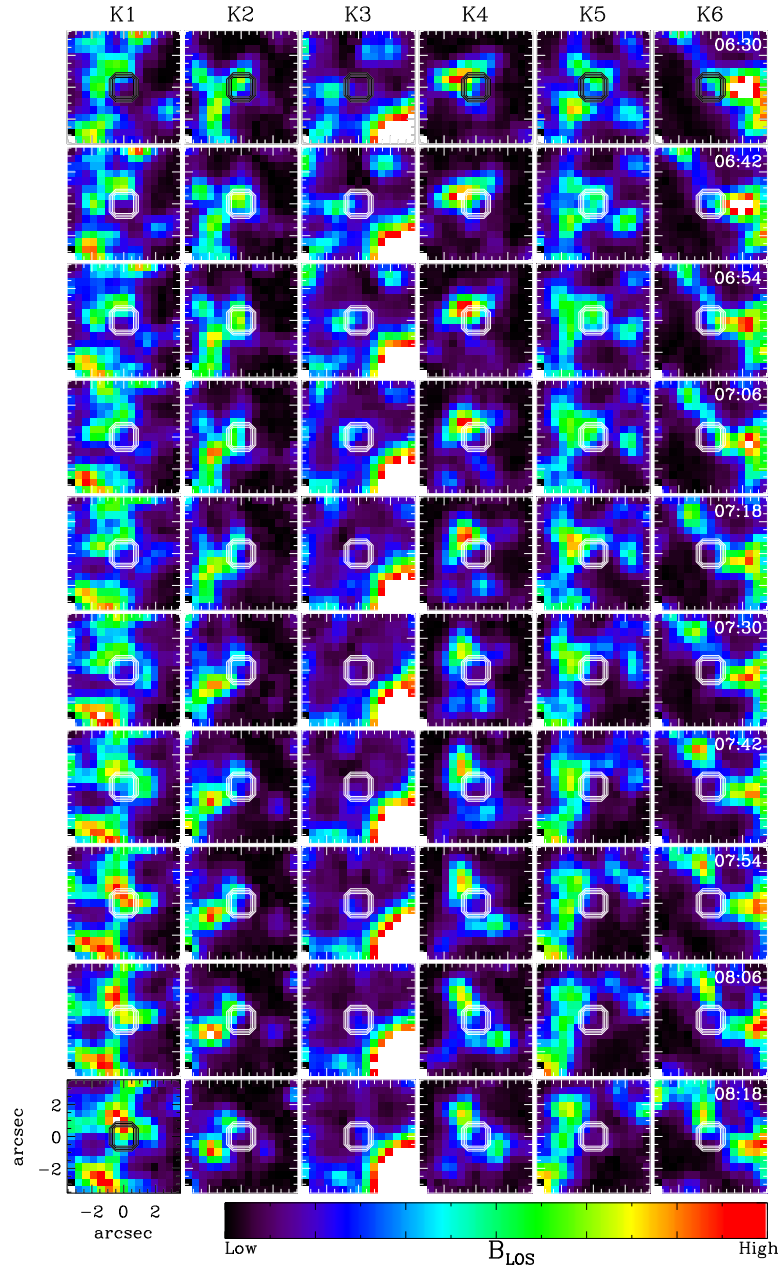


Fig. 6 Mosaic of images showing the time evolution of B_{los} over a grid of 15×15 pixels containing the raster of 3×3 pixels at its center (enclosed by a white box) corresponding to the centroids of the locations ‘K1’, ‘K2’, ‘K3’, ‘K4’, ‘K5’ and ‘K6’ in the active region for the period from 06:30 UT to 08:18 UT at the time interval of 12 min. Each column represents the temporal evolution of B_{los} for a given kernel from top to bottom. The dynamic range of B_{los} is different for the columns (kernels), however within a column the range is the same. For the locations ‘K3’ and ‘K6’, the pixels with high values of B_{los} are saturated in order to enhance the visibility of the morphological evolution of magnetic features within the white boxes. The FOV is $\sim 7.5 \times 7.5 \text{ arcsec}^2$.

For this purpose, we have considered two locations (‘M1’ and ‘M2’) in the active region which show a gradual evolution of B_{los} during the flare, and two locations (‘Q1’ and ‘Q2’) in the quiet Sun. The centroids of these locations are shown by yellow crosses within blue circles in Figure 4. The Carrington heliocentric longitudes and latitudes (in degrees of the aforementioned centroids are as follows:

M1(73.76, 10.96), M2(80.18, 9.61), Q1(67.13, 4.78) and Q2(81.56, 14.05).

In Figure 9, we have plotted the mean B_{los} (left panels) and the mean line-of-sight velocity signals (right panels) after removing the large background gradient over a raster of 3×3 pixels for the aforementioned kernels during the period from 06:00 UT to 10:00 UT on 2013 April 11. In the case of ‘M1’, we observe a gross decrease of $\sim 200 \text{ G}$ in the

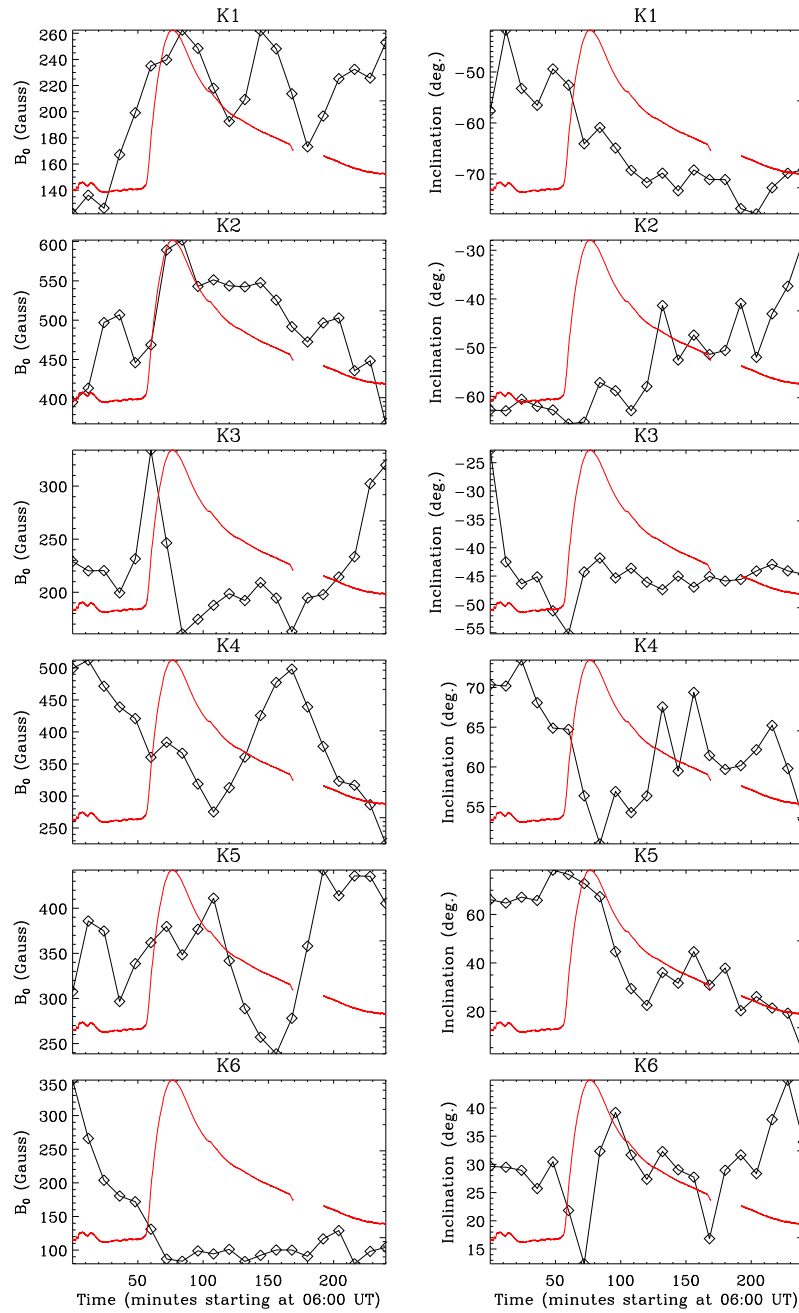


Fig. 7 Plots shown in black lines (with diamonds) in the *left* panels represent the time evolution of the total magnetic field strength (B_0) averaged over a raster of nine pixels in the locations ‘K1’, ‘K2’, ‘K3’, ‘K4’, ‘K5’ and ‘K6’ in the active region during the period 06:00–10:00 UT on 11 April 2013 at the cadence of 12 min. Similarly, the plots shown in black lines (with diamonds) in the *right* panels represent the time evolution of the simultaneous inclination angle (γ) in the aforementioned locations. The B_0 and γ measurements are from HMI. The plots shown in red lines in all the panels represent the evolution of soft X-ray flux in the 1–8 Å energy-band as observed with the *GOES-15*. Here, we notice that both the B_0 and γ show sudden changes in these locations during the flare.

B_{los} whereas ‘M2’ shows a gross decrease of ~ 500 G in the B_{los} during the flare. Here, we do not notice any significant perturbations in the photospheric Doppler signals during the flare in these locations of the active region. In the quiet locations ‘Q1’ and ‘Q2’, the variations in the mean B_{los} are within the noise level of the instrument (~ 10 G) while the mean line-of-sight velocity signals are dominant and show normal evolution during the flare.

In Figure 10, we show the average power spectra of velocity oscillations in these locations for the pre-flare phase (01:00–05:00 UT) and the flare phase (06:00–10:00 UT). In the case of ‘M1’ and ‘M2’, we notice from these velocity power spectra that there is an enhancement of the power of velocity oscillations in the 2 – 5 mHz band during the flare as compared to the pre-flare condition. We also observe that the enhancement in oscillatory power at

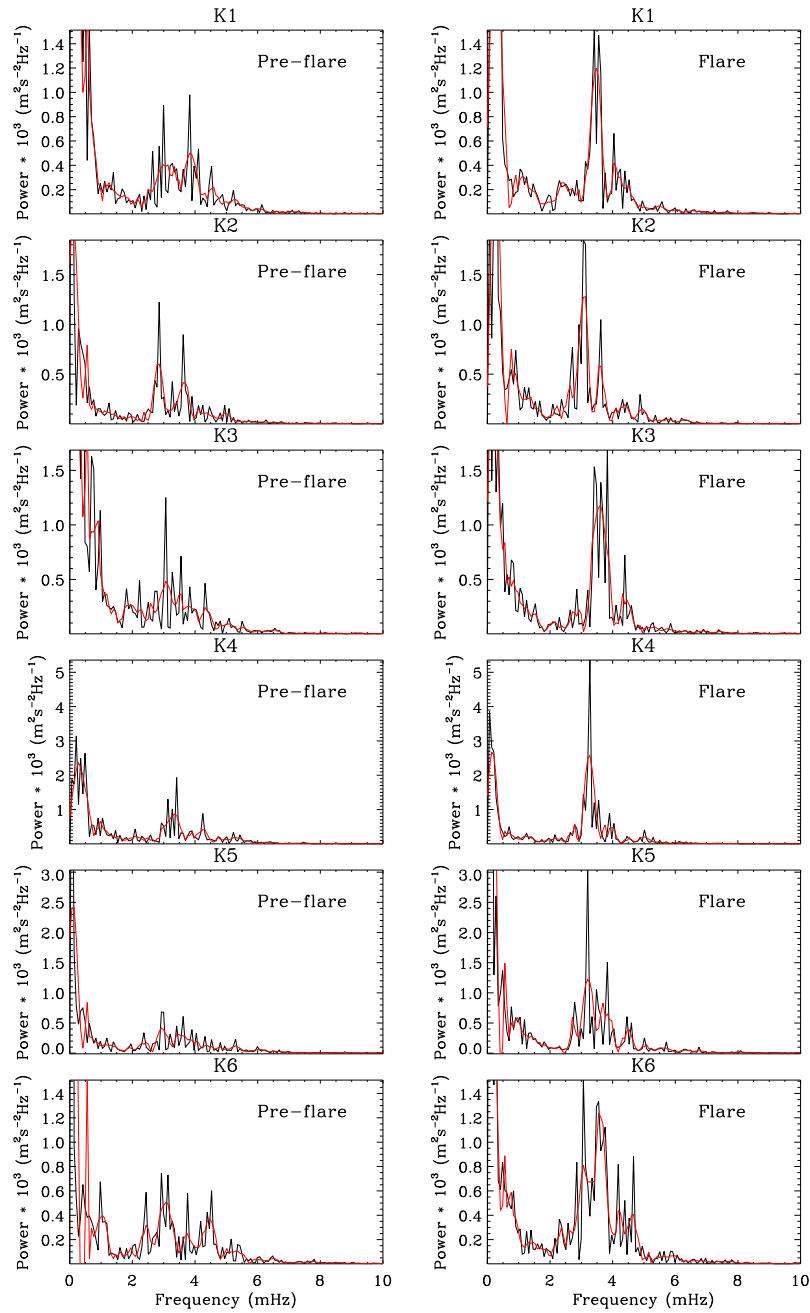


Fig. 8 Plots shown in black lines in the *left* panels represent the average Fourier power spectrum of velocity oscillations estimated over a raster of nine pixels in the locations ‘K1’, ‘K2’, ‘K3’, ‘K4’, ‘K5’ and ‘K6’ in the active region during the period 01:00–05:00 UT on 2013 April 11. Similarly, the plots shown in black lines in the *right* panels represent the average Fourier power spectrum of velocity oscillations estimated over the same raster of nine pixels in the aforementioned locations during the period 06:00–10:00 UT on 2013 April 11. The plots shown in red lines in all the panels represent a smoothing fit (Savitzky-Golay Fit) applied to the original power spectrum to estimate the power envelopes. These plots show that the acoustic power is enhanced in the aforementioned locations in the 2 – 5 mHz frequency band during the flare.

the location ‘M2’ is more as compared to that in the location ‘M1’. Here, it is worth mentioning that during the flare the gross decrease in B_{los} is more at ‘M2’ as compared to that in ‘M1’ and hence this has resulted in relatively more enhancement of oscillatory power at ‘M2’. In the case of ‘Q1’ and ‘Q2’, we do not observe any significant varia-

tions in the power of the velocity oscillations during the flare as compared to the pre-flare condition. These results show that the evolution of magnetic concentrations in the locations ‘M1’ and ‘M2’ is controlling the enhancement of the power of the velocity oscillations in these locations during the flare, while ‘Q1’ and ‘Q2’ remain unaffected

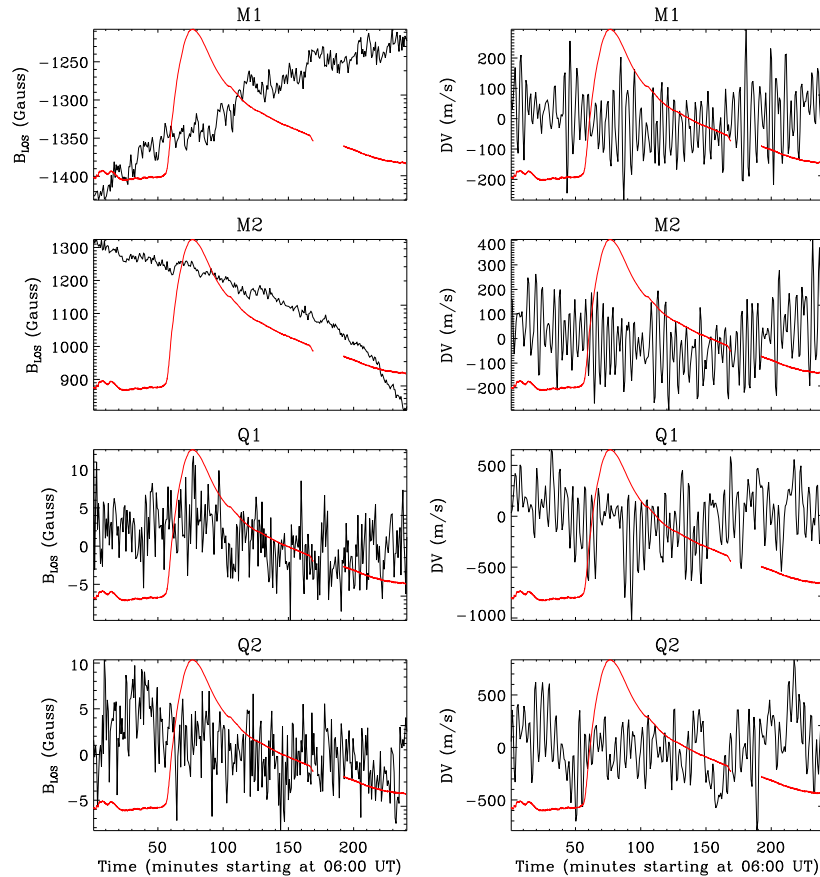


Fig. 9 Same as Fig. 5, but for the locations ‘M1’ and ‘M2’ in the active region, and the locations ‘Q1’ and ‘Q2’ in the quiet Sun. Here, we notice that the line-of-sight photospheric magnetic fields (B_{los}) show gradual evolution in the locations ‘M1’ and ‘M2’ during the flare. We do not observe any significant changes in the photospheric Doppler velocity (DV) in these locations during the flare. In the quiet locations ‘Q1’ and ‘Q2’, the variations in the mean B_{los} are within the noise level of the instrument (~ 10 G) while the DV is dominant and shows normal evolution during the flare.

since they are in the quiet Sun. However, as we have discussed earlier, this assumption is not applicable at the sites of the magnetic-jerks in the active region during the flare. We have observed enhancements in the acoustic power at the locations of magnetic-jerks irrespective of the increase or decrease of B_{los} at these locations during the flare with respect to the pre-flare condition. It is also worth noting that the effect of magnetic-jerks is more pronounced on the power of acoustic oscillations as compared to that due to normal variations in B_{los} at the locations ‘M1’ and ‘M2’.

Another important point is that we do not observe any instantaneous large velocity signal appearing right at the time of the impulsive phase of the flare as has been seen in the active regions during several major X-class flares. Such large spiky velocity and magnetic signals may also appear due to distortions in the line profile in the flaring regions. In our case, the identified locations are in the vicinity of the flare-ribbons and also away from the sites of these ribbons. We observe relatively enhanced photospheric velocity signals following the phenomena of sudden and persistent changes seen in B_{los} in the active region and this is the reason why these lead to the enhancement in the gross

power of the acoustic spectra for the flare phase covering the magnetic-jerks, as compared to the pre-flare phase.

3.3 Analysis of $H\alpha$ Intensity Oscillations in the Active Region using GONG++ Data

We have a nearly simultaneous sequence of chromospheric observations consisting of full-disk $H\alpha$ filtergrams available from GONG++ along with the above magnetic and velocity field observations from HMI. The availability of these $H\alpha$ observations from GONG++ provides the opportunity to study the possible changes in $H\alpha$ intensity oscillations driven by the aforementioned “magnetic-jerk” in the active region appearing during the flare. We have reasonably good quality full-disk $H\alpha$ images available from the GONG++ instrument for the period from 03:01 UT to 09:31 UT on 2013 April 11 at a cadence of one minute. The sequence of these $H\alpha$ images, taken every minute, is derotated and registered with respect to the image taken at 03:01 UT with an accuracy of $0.1''$. A grid with size $\sim 290 \times 193$ arcsec² consisting of the active region is selected from each of the derotated and registered sequence

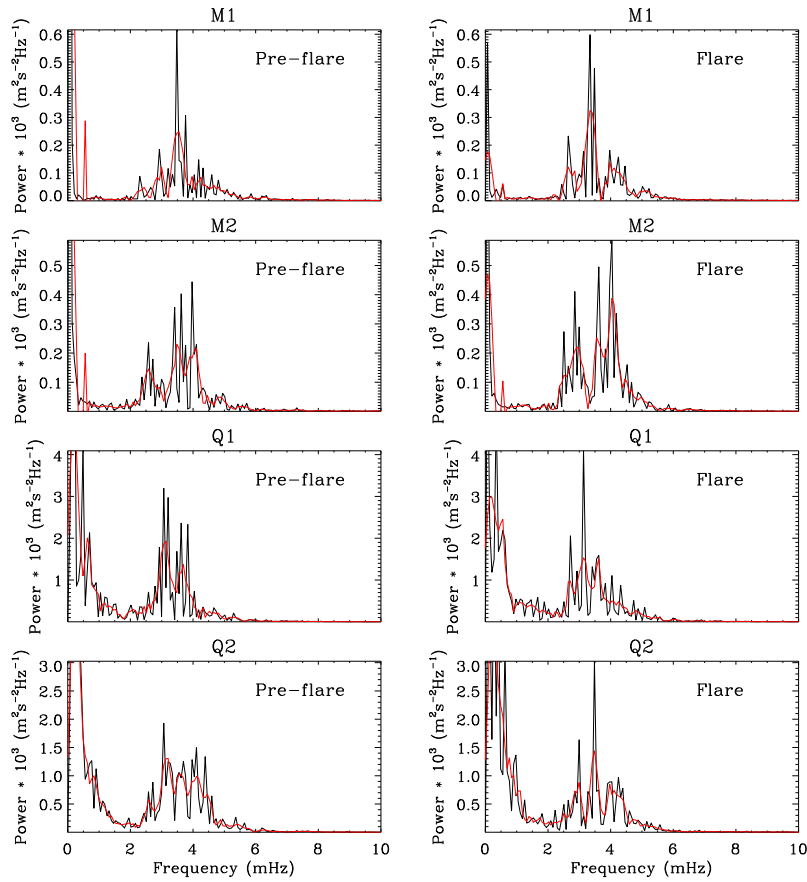


Fig. 10 Same as Fig. 8, but for the locations ‘M1’ and ‘M2’ in the active region and the locations ‘Q1’ and ‘Q2’ in the quiet Sun. Here, we notice that the power of velocity oscillations is enhanced in the locations ‘M1’ and ‘M2’ in the 2 – 5 mHz frequency band during the flare. This enhancement in power is more for ‘M2’ as compared to that for ‘M1’ which could be attributed to the amount of reduction in the line-of-sight photospheric magnetic fields in the active region during the flare. In the case of ‘Q1’ and ‘Q2’, we do not observe any significant variations in the power of velocity oscillations during the flare, being in the quiet Sun.

of full-disk $H\alpha$ images. The sequence of these images is aligned with respect to the image at 03:01 UT using a Fast Fourier transform based cross-correlation algorithm with an accuracy of $0.1''$. These registered images are re-scaled to the spatial scale of 0.5 arcsec per pixel in order to match the pixel scale of HMI data. The re-scaled image sequence is then co-aligned with respect to the field-of-view of the grid of magnetic and velocity images from HMI used in our analysis. The sequence of these co-aligned grids of $H\alpha$ images is segregated into two parts for our analysis: the pre-flare phase (03:01–06:01 UT) and the flare phase (06:31–09:31 UT). Now, it would be reasonable to consider that the locations of the “magnetic-jerk” seen in the photosphere would not be the same as in the chromosphere due to the inclination of the magnetic field lines. Hence, we have scanned through the pixels around the centroids of the grid of 3×3 pixels in the locations ‘K1’, ‘K2’, ‘K3’, ‘K4’, ‘K5’ and ‘K6’ as considered in the case of HMI magnetic and velocity images in order to find the best locations showing any “magnetic-jerk” driven chromospheric oscillations in the active region during the flare. Following this, we found such locations in these $H\alpha$ images which show enhancement of power in intensity oscillations dur-

ing the flare and are situated slightly away (within $2''$) from the aforementioned centroids of the sites of magnetic-jerks in the photospheric magnetograms in the locations ‘K1’, ‘K2’, ‘K3’, ‘K4’, ‘K5’ and ‘K6’. However, these new locations seen in $H\alpha$ images do not exactly match the deviations as estimated ($\approx h \cdot \tan(\gamma)$; h = difference in the average formation heights of the lines) from the inclination angles (γ) available from the photospheric vector magnetograms from HMI. The most important reason for this mismatch could be the canopy effect in the chromosphere, where the magnetic field lines spread out and become more tilted in general than in the photosphere. However, the other probable sources of errors could be as follows: (i) the seeing effects in the $H\alpha$ ground-based observations obtained from GONG++ as compared with the space-based observations with HMI, (ii) the errors in the co-alignment of images from the two different instruments with different spatial resolutions, and (iii) the difference in the available observational cadence of B_{los} (45 s) and γ (12 min). In Figure 11, we show the evolution of normalized $H\alpha$ light curves averaged over a grid of 3×3 pixels in the new locations within ‘K1’, ‘K2’, ‘K3’, ‘K4’, ‘K5’ and ‘K6’ in the active region during the phases of pre-flare

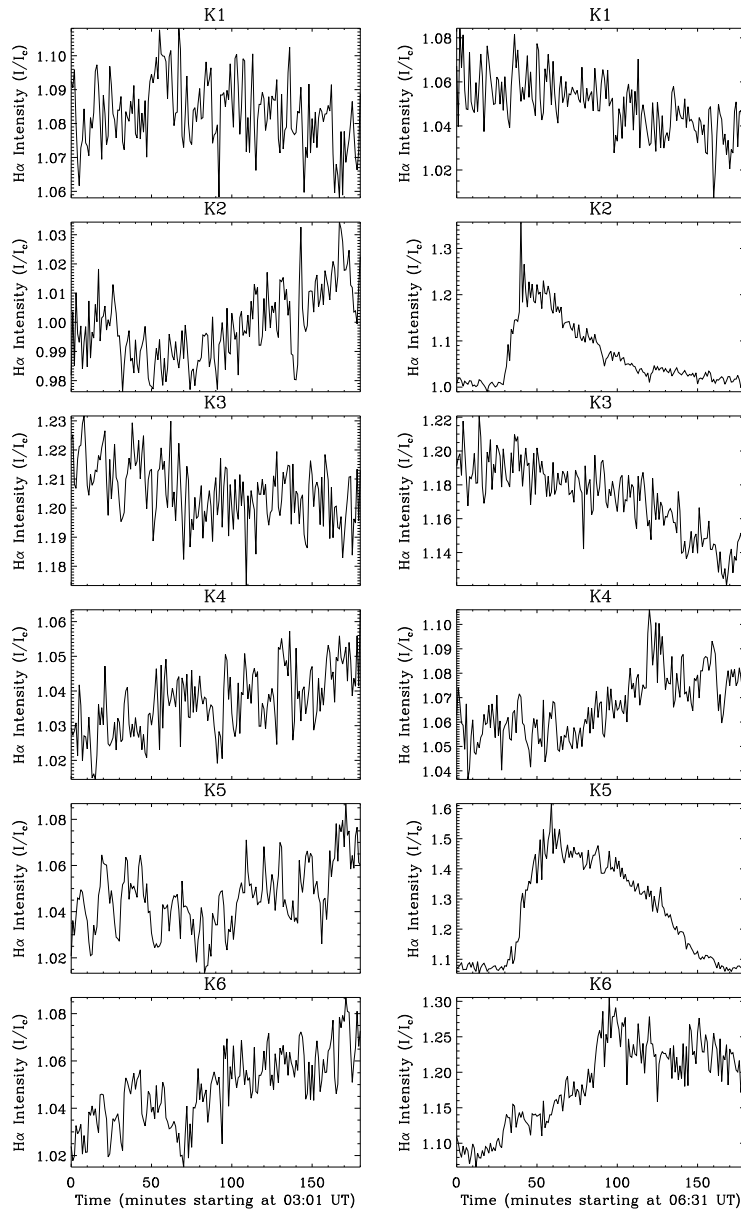


Fig. 11 Plots shown in black lines in the *left* panels represent the time evolution of normalized H α light curves averaged over a raster of nine pixels within the locations ‘K1’, ‘K2’, ‘K3’, ‘K4’, ‘K5’ and ‘K6’ in the active region during the period 03:01–06:01 UT on 2013 April 11 (pre-flare condition). Similarly, the plots shown in black lines in the *right* panels represent the time evolution of normalized H α light curves averaged over the same rasters of nine pixels within the aforementioned locations during the period 06:31–09:31 UT on 2013 April 11 (spanning the flare). Here, the observational cadence is one minute.

and flare conditions. These H α light curves exhibit quasi-periodic intensity variations which are similar to the observations of Wang et al. (2000) for a C5.7 flare that occurred in the solar active region NOAA 8673 on 1999 August 23. Wang et al. (2000) used high-resolution H α observations of this C-class flare obtained at BBSO. Resembling the velocity power spectrum, we have estimated the Fourier power spectrum of the H α intensity oscillations in each of the individual pixels in the new grids of 3×3 pixels in the aforementioned locations and constructed average power spectra for the pre-flare and flare phases (c.f., Fig. 12). It

is evident from these power spectra that there is enhancement of power in chromospheric intensity oscillations in these locations during the flare as compared to the pre-flare condition.

4 DISCUSSION AND CONCLUSIONS

We have investigated the photospheric magnetic and velocity field changes in the active region NOAA 11719 during a large two-ribbon flare (of class M6.5) that occurred on 2013 April 11, using high-quality observations obtained from the HMI instrument onboard the *SDO* spacecraft.

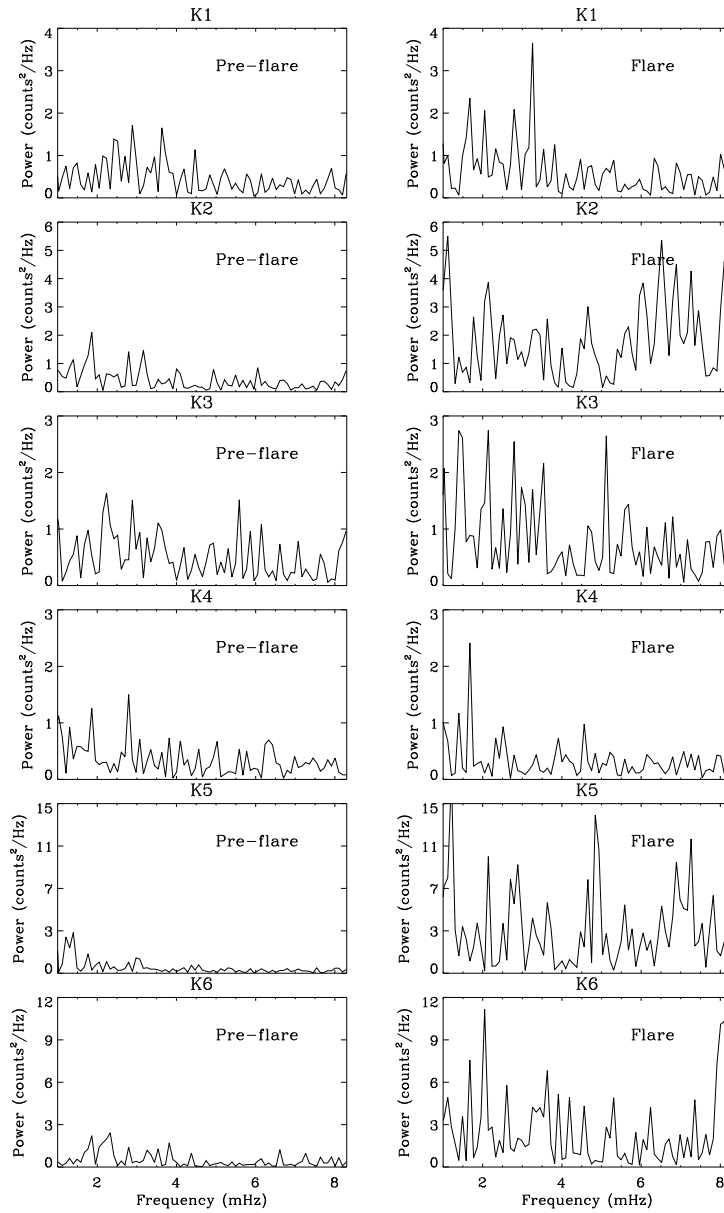


Fig. 12 Plots shown in black lines in the *left* panels represent the average Fourier power spectrum of $H\alpha$ intensity oscillations estimated over a raster of nine pixels within the locations ‘K1’, ‘K2’, ‘K3’, ‘K4’, ‘K5’ and ‘K6’ in the active region during the period 03:01–06:01 UT on 2013 April 11 (pre-flare condition). Similarly, the plots shown in black lines in the *right* panels represent the average Fourier power spectrum of $H\alpha$ intensity oscillations estimated over the same rasters of nine pixels within the aforementioned locations of the active region for the period 06:31–09:31 UT on 2013 April 11 (spanning the flare). It is evident that the power of $H\alpha$ intensity oscillations is enhanced in the aforementioned locations during the flare.

Accompanying these photospheric observations, we have also analyzed the nearly simultaneous chromospheric $H\alpha$ observations from the GONG++ instrument in order to understand any possible inter-linked physical process taking place between the different layers in the solar atmosphere. The chief findings of our investigations and the interpretations of our results are as follows:

- (i) The analysis of the line-of-sight magnetic fields (B_{los}) from HMI shows sudden and persistent magnetic field changes at different locations of the active region during the flare. These sites (‘K1’, ‘K2’, ‘K3’, ‘K4’, ‘K5’

and ‘K6’) are located in the vicinity of the $H\alpha$ flare-ribbons, as well as away from the flare-ribbons in the active region. We also observe that these abrupt changes in (B_{los}) appear before the onset of flare, as well as during the flare, and are seen mostly in the weak to moderate magnetic field concentrations in the active region. Burtseva et al. (2015) analyzed several X-class flares and have reported abrupt magnetic field changes which take place before or around the start time of the flare. They have also shown that these field changes and the footpoints of the hard X-ray emission

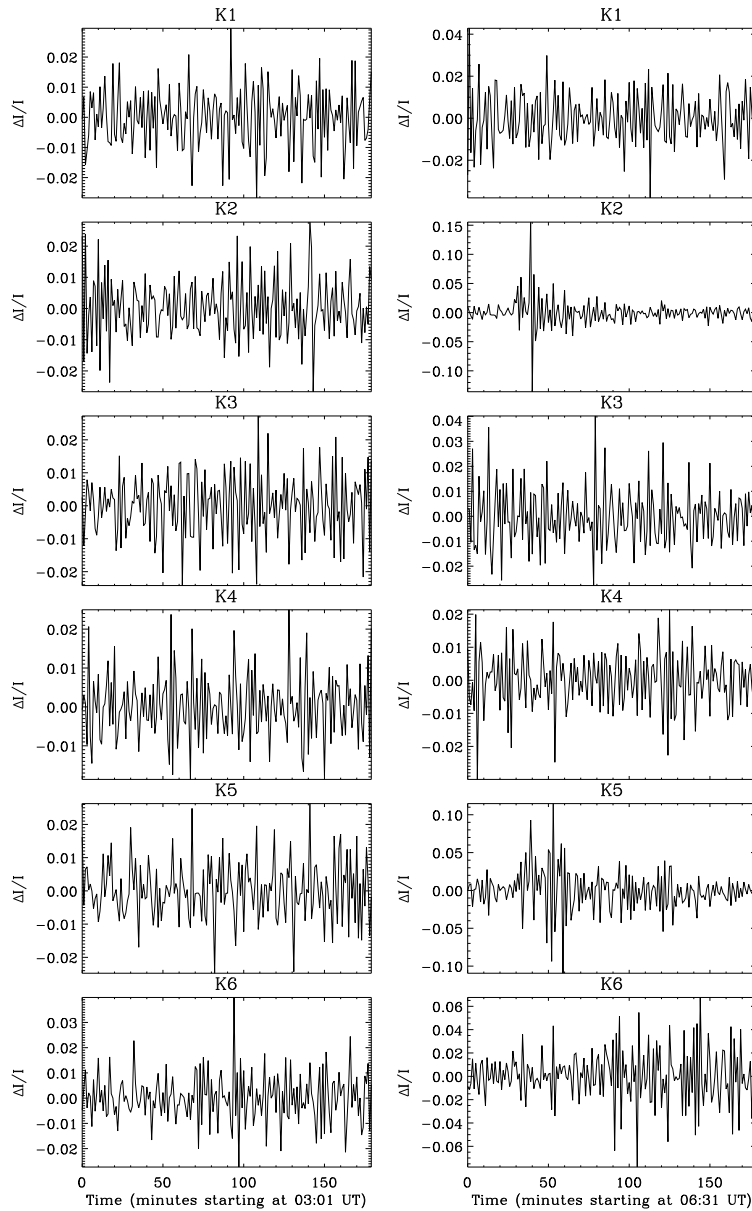


Fig. 13 Plots shown in black lines in the *left* panels represent time evolution of $\Delta I/I$ (extracted from $H\alpha$ light curves) averaged over a raster of nine pixels within the locations ‘K1’, ‘K2’, ‘K3’, ‘K4’, ‘K5’ and ‘K6’ in the active region during the period 03:01–06:01 UT on 2013 April 11 (pre-flare condition). Similarly, the plots shown in black lines in the *right* panels represent the time evolution of $\Delta I/I$ (extracted from $H\alpha$ light curves) averaged over the same rasters of nine pixels within the aforementioned locations during the period 06:31–09:31 UT on 2013 April 11 (spanning the flare). The oscillatory behavior of the quantity $\Delta I/I$ (the proxy for chromospheric velocity amplitude) is clearly seen in these plots.

during the flare are not always co-spatial. Our results show that the amount of change in B_{los} is between 100 G and 200 G taking place within the time scales of 10 min, which are similar to the findings of Sudol & Harvey (2005) and Petrie & Sudol (2010). However, the abrupt changes in B_{los} in our observations are “persistent” but not “permanent” changes in longitudinal magnetic fields as have been found by Sudol & Harvey (2005) and Petrie & Sudol (2010) for other flare events. From our analysis related to the morpho-

logical evolution of B_{los} at these locations, we conjecture that the sudden changes in the B_{los} observed at these locations could be due to the process of fast re-organization of the coronal magnetic fields during the flare resulting into fast changes in the directions of photospheric vector fields. We have also analyzed the vector magnetic field data available from HMI which show that the sudden changes seen in the B_{los} are accompanied with the coincident sudden changes in B_0 and γ at these locations in the active region. There

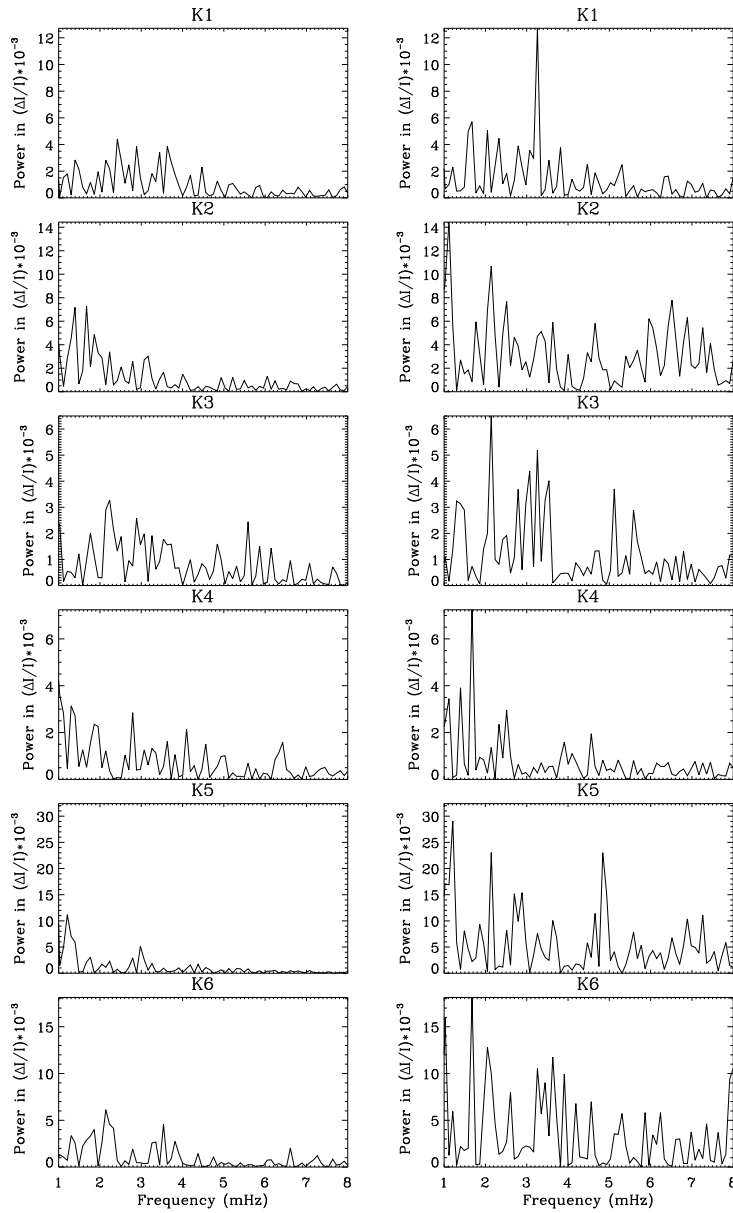


Fig. 14 Plots shown in black lines in the *left* panels represent the average Fourier power spectrum of $\Delta I/I$ (extracted from $H\alpha$ light curves) estimated over a raster of nine pixels within the locations ‘K1’, ‘K2’, ‘K3’, ‘K4’, ‘K5’ and ‘K6’ in the active region during the period 03:01–06:01 UT on 2013 April 11 (pre-flare condition). Similarly, the plots shown in black lines in the *right* panels represent the average Fourier power spectrum of $\Delta I/I$ (extracted from $H\alpha$ light curves) estimated over the same rasters of nine pixels within the aforementioned locations of the active region for the period 06:31–09:31 UT on 2013 April 11 (spanning the flare). It is evident that the power of $\Delta I/I$ oscillations (the proxy for chromospheric velocity oscillations) is enhanced in the aforementioned locations during the flare.

has always been a concern regarding the distortions in the line profile affecting the observations of magnetic and velocity fields in the active region during the impulsive phase of the large flares (Qiu & Gary 2003). However, this speculation could be applicable for the locations situated within the flare-ribbons or the hard X-ray footpoints. In such cases, large short-lived changes appear in the magnetic and velocity fields during the flare. In our case, some of the affected locations (‘K1’, ‘K3’ and ‘K4’) are away from the $H\alpha$ flare-

ribbons and hence these are free from the possible effect of distortions in the line profile. On the other hand, for the locations in the vicinity of the $H\alpha$ flare-ribbons (‘K2’, ‘K5’ and ‘K6’), we do not observe any large spiky signals appearing for short times in the B_{los} and Doppler velocity signals at these locations. It is also important to note that the profiles of B_{los} and Doppler velocity for all the locations ‘K1’, ‘K2’, ‘K3’, ‘K4’, ‘K5’ and ‘K6’ appear similar in nature. Hence, we suggest that the sudden changes appearing in B_{los} and the

subsequent perturbations in the Doppler velocity signals in the aforementioned locations are real changes happening in the active region during the flare.

- (ii) It is believed that the Lorentz-force-transients associated with the “magnetic-jerk” can drive localized seismic waves in the solar photosphere (Hudson et al. 2008; Fisher et al. 2012). Hence, we have analyzed the HMI Dopplergrams for the photospheric velocity signals in the locations ‘K1’, ‘K2’, ‘K3’, ‘K4’, ‘K5’ and ‘K6’ for the epochs before and spanning the flare. For this purpose, we have estimated the Fourier power spectrum of these velocity oscillations in the aforementioned locations. It is observed that the power of velocity oscillations is enhanced in the locations of magnetic-jerks spanning the flare as compared to the pre-flare condition. This enhancement is found for all the sites of magnetic-jerks in the active region during the flare. There are other physical processes responsible for driving oscillations in the solar atmosphere during the flare, mainly the chromospheric shocks propagating through the photosphere into the solar interior (Fisher et al. 1985) or the high-energy particle beam impinging on the solar photosphere (Venkatakrishnan et al. 2008 and references therein). However, this is applicable for the situation when the affected areas are within the hard X-ray footpoints or $H\alpha$ flare kernels. In our case, the affected locations are situated in the vicinity of the flare-ribbons and also far away from the flare-ribbons in the active region, hence this indicates that magnetic-jerks have certainly driven these localized photospheric velocity oscillations. A general estimate is that the transient Lorentz forces with magnitude $\sim 10^{22}$ dynes (Hudson et al. 2008; Fisher et al. 2012) associated with these magnetic-jerks could be responsible for driving localized seismic waves in the solar photosphere. Following Fisher et al. (2012), we estimate the approximate transient Lorentz force ($B_{\text{los}} \cdot \delta B_{\text{los}} \cdot A / 4\pi$) corresponding to the sites of the magnetic-jerks in the active region during this flare event. In our case, the mean value of the line-of-sight magnetic field changes (δB_{los}) is ~ 150 G and the mean value of B_{los} at these locations is ~ 300 G over an area (A) of $\sim 10^{16}$ cm² as obtained from HMI magnetograms in the locations of the magnetic-jerks. Hence, the approximate estimate of the transient Lorentz force at these sites of magnetic-jerks turns out to be $\sim 10^{19}$ dynes. This is a lower available budget of the transient Lorentz force as compared to the required magnitude of the force for driving the localized seismic waves. It can be noted that the expression of Fisher et al. (2012) for estimating the transient Lorentz force is applicable for strong magnetic field regions (≥ 1 kG optimally at the $\tau = 1$ opacity layer at the wavelength 5000 Å) and also approximated under some theoretical assumptions (for a detailed discussion, please refer to Petrie 2014). In our case, the sites of magnetic-jerks are located in weak to moderate

field regions (≤ 500 G) and also our estimate suffers from the non-availability of all the vector components simultaneously. Hence, the above constraints could be the reason for the deficit in the budget of transient force appearing in our estimation, by using the expression of Fisher et al. (2012) under approximations. However, we do observe enhancements in the power of velocity oscillations in the locations of the magnetic-jerks in the active region during the flare. In our observations, the average change in the amplitude of localized velocity oscillations (Δv) associated with the magnetic-jerks is ~ 200 m s⁻¹. Hence, the estimate of the transient force required to drive these acoustic oscillations could be $\approx \rho(\Delta v^2)A$, where ‘ ρ ’ is the mean density of the solar photosphere ($\sim 2 \times 10^{-7}$ g cm⁻³). This yields a required budget of the driving force of $\sim 8 \times 10^{17}$ dynes against the available budget of the transient force of $\sim 10^{19}$ dynes as estimated from the magnetic-jerks. Thus, from the aforementioned calculation it appears that the magnetic-jerks at the locations ‘K1’, ‘K2’, ‘K3’, ‘K4’, ‘K5’ and ‘K6’ are capable of driving the localized photospheric acoustic oscillations.

- (iii) Using the $H\alpha$ chromospheric observations of this flare from the GONG++ instrument, we have analyzed the changes in the $H\alpha$ intensity oscillations in the corresponding locations of the magnetic-jerks in the active region during the flare. The motivation of this analysis is to study the possible inter-linking physical processes between the different layers of the solar atmosphere. For this purpose, we have applied a Fourier transform to the $H\alpha$ intensity oscillations in these affected locations for the epochs before and spanning the flare. It is observed that there is enhancement in the power of $H\alpha$ intensity oscillations in these locations during the flare. The power enhancement is seen at different frequencies for the kernels ‘K1’, ‘K2’, ‘K3’, ‘K4’, ‘K5’ and ‘K6’. These findings are similar to the results of Wang et al. (2000) in the case of flare driven $H\alpha$ intensity oscillations. In our case, some of the locations are in the vicinity of the flare loops and hence the flare would have mainly contributed to the enhancement of the chromospheric intensity oscillations in these locations. However, for the locations which are away from the flare-ribbons, the contribution of the magnetic-jerks in driving these oscillations cannot be disregarded. We investigate this further by extracting the approximate estimates of chromospheric velocity amplitudes from $\Delta I/I$ of the $H\alpha$ light curves assuming that these intensity oscillations are wholly caused by the Doppler shift in the $H\alpha$ line due to the motion of chromospheric plasma. Under this assumption, the quantity $\Delta I/I$ could be the proxy for the chromospheric velocity amplitude. We plot this quantity for all the locations ‘K1’, ‘K2’, ‘K3’, ‘K4’, ‘K5’ and ‘K6’ in Figure 13. It is seen from these plots that the quantity $\Delta I/I$ shows oscillatory behavior at all the aforemen-

tioned locations for the epochs before and spanning the flare. We do observe some spikes in the temporal behavior of $\Delta I/I$ spanning the flare for the locations ‘K2’, ‘K5’ and ‘K6’. However, they could be attributed to the effect of the flare as these locations are in the vicinity of $H\alpha$ flare-ribbons. We have also estimated the Fourier power spectrum of the variations in $\Delta I/I$ for all the locations (‘K1’, ‘K2’, ‘K3’, ‘K4’, ‘K5’ and ‘K6’) for the pre-flare phase (03:01–06:01 UT) and the flare phase (06:31–09:31 UT) as shown in Figure 14. It is observed that these power spectra show a general enhancement in the oscillatory power during the flare as compared to the pre-flare phase for all these locations. However, this effect is more for the locations in the vicinity of the $H\alpha$ flare loops (‘K2’, ‘K5’ and ‘K6’) as compared to the locations away from the flare loops (‘K1’, ‘K3’ and ‘K4’). Thus, our results indicate that these magnetic-jerks could also power the chromospheric oscillations, apart from the localized photospheric oscillations.

These magnetically driven oscillations in the active regions are important for understanding the transport of acoustic energy from the photospheric levels to the higher solar atmospheric layers.

Acknowledgements We are thankful to the anonymous referee for constructive comments and suggestions that improved the discussions and presentation of our work in this paper. We acknowledge the use of data from the HMI instrument onboard the *SDO* spacecraft. The *SDO* is a mission of NASA aimed at understanding the causes of solar variability and its impacts on Earth. Our sincere thanks go to the HMI team for providing the tracked magnetic and velocity data as per our requirement. This work utilizes the Global Oscillation Network Group (GONG) data obtained by the NSO Integrated Synoptic Program (NISP), managed by the National Solar Observatory, which is operated by AURA, Inc. under a cooperative agreement with the National Science Foundation. Thanks to the GONG++ team for providing the processed $H\alpha$ observations. We also acknowledge the use of data from the *GOES-15* space mission.

References

- Burtseva, O., Martínez-Oliveros, J. C., Petrie, G. J. D., & Pevtsov, A. A. 2015, *ApJ*, 806, 173
- Domingo, V., Fleck, B., & Poland, A. I. 1995, *Sol. Phys.*, 162, 1
- Fisher, G. H., Canfield, R. C., & McClymont, A. N. 1985, *ApJ*, 289, 425
- Fisher, G. H., Bercik, D. J., Welsch, B. T., & Hudson, H. S. 2012, *Sol. Phys.*, 277, 59
- Harvey, J. 1986, in *Small Scale Magnetic Flux Concentrations in the Solar Photosphere*, eds. W. Deinzer, M. Knölker, & H. H. Voigt (Göttingen: Vandenhoeck & Rupprecht), 25
- Harvey, J., & GONG Instrument Team. 1995, in *Astronomical Society of the Pacific Conference Series*, 76, GONG 1994.
- Helio- and Astro-Seismology from the Earth and Space, eds. R. K. Ulrich, E. J. Rhodes, Jr., & W. Dappen, 432
- Harvey, J. W., Hill, F., Hubbard, R. P., et al. 1996, *Science*, 272, 1284
- Harvey, J., Tucker, R., & Britanik, L. 1998, in *ESA Special Publication*, 418, *Structure and Dynamics of the Interior of the Sun and Sun-like Stars*, ed. S. Korzennik, 209
- Harvey, J. W., Bolding, J., Clark, R., et al. 2011, in *Bulletin of the American Astronomical Society*, 43, *AAS/Solar Physics Division Abstracts #42*, 17.45
- Hudson, H. S., Fisher, G. H., & Welsch, B. T. 2008, in *Astronomical Society of the Pacific Conference Series*, 383, *Subsurface and Atmospheric Influences on Solar Activity*, eds. R. Howe, R. W. Komm, K. S. Balasubramaniam, & G. J. D. Petrie, 221
- Kaiser, M. L., Kucera, T. A., Davila, J. M., et al. 2008, *Space Sci. Rev.*, 136, 5
- Kosovichev, A. G., & Zharkova, V. V. 2001, *ApJ*, 550, L105
- Kosugi, T., Matsuzaki, K., Sakao, T., et al. 2007, *Sol. Phys.*, 243, 3
- Kumar, B., Venkatakrishnan, P., Mathur, S., Tiwari, S. K., & García, R. A. 2011, *ApJ*, 743, 29
- Lin, R. P., Dennis, B. R., Hurford, G. J., et al. 2002, *Sol. Phys.*, 210, 3
- Nakajima, H., Sekiguchi, H., Sawa, M., Kai, K., & Kawashima, S. 1985, *PASJ*, 37, 163
- Patterson, A., & Zirin, H. 1981, *ApJ*, 243, L99
- Patterson, A. 1984, *ApJ*, 280, 884
- Pesnell, W. D., Thompson, B. J., & Chamberlin, P. C. 2012, *Sol. Phys.*, 275, 3
- Petrie, G. J. D., & Sudol, J. J. 2010, *ApJ*, 724, 1218
- Petrie, G. J. D. 2014, *Sol. Phys.*, 289, 3663
- Press, W. H., Teukolsky, S. A., Vetterling, W. T., & Flannery, B. P. 1992, *Numerical recipes in FORTRAN. The Art of Scientific Computing* (Cambridge: Cambridge University Press)
- Qiu, J., & Gary, D. E. 2003, *ApJ*, 599, 615
- Scherrer, P. H., Bogart, R. S., Bush, R. I., et al. 1995, *Sol. Phys.*, 162, 129
- Schou, J., Scherrer, P. H., Bush, R. I., et al. 2012, *Sol. Phys.*, 275, 229
- Sudol, J. J., & Harvey, J. W. 2005, *ApJ*, 635, 647
- Venkatakrishnan, P., Kumar, B., & Uddin, W. 2008, *MNRAS*, 387, L69
- Wang, H. 1992, *Sol. Phys.*, 140, 85
- Wang, H., Ewell, Jr., M. W., Zirin, H., & Ai, G. 1994, *ApJ*, 424, 436
- Wang, H., Qiu, J., Denker, C., et al. 2000, *ApJ*, 542, 1080
- Wang, H., Spirock, T. J., Qiu, J., et al. 2002, *ApJ*, 576, 497